Nanotip acetylcholine biosensor reveals cholinergic differentiated SH-SY5Y cells release partial vesicle content during exocytosis

Bioelectrochemistry 171 (2026) 109260

Contents lists available at ScienceDirect

Bioelectrochemistry

journal homepage: www.journals.elsevier.com/bioelectrochemistry

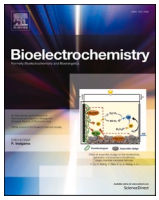

Nanotip acetylcholine biosensor reveals cholinergic differentiated SH-SY5Y cells release partial vesicle content during exocytosis☆

Yuanmo Wang [a,1,2], Ajay Pradhan [b,1,3], Pankaj Gupta [a,4], Jörg Hanrieder [b,d,5], Henrik Zetterberg [b,c,d,e,f,g,6], Ann-Sofie Cans [a,*,7]

[a] Department of Chemistry and Chemical Engineering, Chalmers University of Technology, Kemigården 4, SE-412 96 Gothenburg, Sweden
[b] Department of Psychiatry and Neurochemistry, Institute of Neuroscience & Physiology, the Sahlgrenska Academy at the University of Gothenburg, Mölndal, Sweden
[c] Clinical Neurochemistry Laboratory, Sahlgrenska University Hospital, Mölndal, Sweden
[d] Department of Neurodegenerative Disease, UCL Institute of Neurology, Queen Square, London, UK
[e] UK Dementia Research Institute at UCL, London, UK
[f] Hong Kong Center for Neurodegenerative Diseases, Clear Water Bay, Hong Kong, China
[g] Wisconsin Alzheimer's Disease Research Center, University of Wisconsin School of Medicine and Public Health, University of Wisconsin-Madison, Madison, WI, USA

ARTICLE INFO

Keywords:
Acetylcholine
Carbon fiber nanotip electrode
Ultrafast
Biosensor
Exocytosis
Quantal storage
Vesicle neurotransmitter analysis
Amperometry
SH-SY5Y cells
Full exocytosis
Partial exocytosis

ABSTRACT

Acetylcholine (ACh) is a central neurotransmitter in cognitive function, motor control, and synaptic modulation, yet its electrochemical inactivity and the rapid kinetics of exocytosis have hindered real-time quantal measurements. Micrometer-scale enzymatic ACh biosensors previously enabled sub-millisecond extracellular recordings but were too large for synaptic positioning and intracellular recordings. Here we present a short, ultrafast and low-noise amperometric ACh biosensor based on a needle-shaped carbon fiber nanotip electrode functionalized with gold nanoparticles and enzymes. The miniaturized geometry allows precise placement at neurite release sites and minimally invasive insertion into the cell cytoplasm, enabling high-temporal resolution monitoring of presynaptic exocytosis together with quantification of intracellular ACh vesicle content. We applied this platform to differentiated human cholinergic SH-SY5Y neuroblastoma cells, an established yet underutilized cell model for cholinergic signaling. The nanotip sensor successfully captured amperometric spikes from both intracellular vesicle burst events and presynaptic ACh release. Intracellular events released a larger amount of ACh than presynaptic exocytosis events, indicating a predominance of partial exocytosis mode in these cells. These results demonstrate the nanotip ACh biosensor as a unique tool for probing fusion pore dynamics at subcellular resolution and for providing quantitative insight into the quantal nature of cholinergic signaling in human neuronal models.

1. Introduction

Acetylcholine (ACh) is a major excitatory neurotransmitter that plays essential roles in both the central and peripheral nervous systems [1]. In the periphery, it regulates heart rate and drives skeletal muscle contraction [1,2], while in the central nervous system, it contributes to cognitive function and modulates activity at glutamatergic and GABAergic synapses [2,3]. Dysregulation of cholinergic signaling has been associated with various neurological and psychiatric disorders, including Alzheimer's disease and schizophrenia [4]. Therefore, a

☆ This article is part of a Special issue entitled: 'Monitoring brain chemistry' published in Bioelectrochemistry.

* Corresponding authors.
E-mail address: cans@chalmers.se (A.-S. Cans).
[1] These authors contributed equally to this work
[2] https://orcid.org/0000-0001-7098-6088.
[3] https://orcid.org/0009-0003-6429-2735.
[4] https://orcid.org/0000-0001-7689-4352.
[5] https://orcid.org/0000-0001-6059-198X.
[6] https://orcid.org/0000-0003-3930-4354.
[7] https://orcid.org/0000-0002-3059-2399.

https://doi.org/10.1016/j.bioelechem.2026.109260
Received 30 September 2025; Received in revised form 20 February 2026; Accepted 25 February 2026
Available online 26 February 2026

detailed understanding of ACh storage and release dynamics is critical for modeling both healthy and pathological conditions. For example, in Alzheimer's disease, in addition to the well-documented excessive loss of cholinergic neurons at later stages of the disease, impaired synthesis of ACh has also been reported, likely resulting in aberrant quantal content and lower release [5]. While in the case of disorders like Lambert-Eaton myasthenic syndrome, the vesicular release mechanism is directly affected [6]. Differentiating between stored ACh content and the amount actually released is essential, as studying release alone provides an incomplete picture. Traditional methods like vesicle isolation fall short in this context, as they expose vesicles to non-physiological conditions that can affect integrity and content [7]. Therefore, cell-based systems capable of preserving the native intracellular environment are indispensable.

To enable such mechanistic studies, particularly in a human-relevant system, human SH-SY5Y neuroblastoma cells and their differentiated phenotypes have been demonstrated as a widely used and promising in vitro model for studying neurotransmission and neurodegenerative disease mechanisms [8]. These cells have also been reliably induced into a cholinergic phenotype, providing a human-relevant alternative to rodent-derived primary neurons and non-neuronal secretory cells such as chromaffin or PC12 cells. Unlike chromaffin and PC12 cells, which release catecholaminergic transmitters via large dense-core vesicles, differentiated cholinergic SH-SY5Y cells utilize small clear-core vesicles for ACh storage, closely mimicking neuronal ACh release [9]. While human iPSC-derived neurons are considered the gold standard for disease modeling, they are often impractical for basic research due to complex and time-consuming protocols, as well as variability in differentiation efficiency. In contrast, immortalized human cell lines like SH-SY5Y offer greater accessibility and consistency, making them particularly suitable for early-stage mechanistic studies of cholinergic signaling.

Studying ACh dynamics in cellular models is technically challenging because ACh is electrochemically inactive and cannot be directly detected by standard electrochemical techniques, including ultrafast amperometry. This presents a significant limitation for monitoring its real-time release during synaptic transmission, which occurs via exocytosis on the millisecond or even sub-millisecond timescale [9]. Accurate detection therefore requires biosensors with not only high sensitivity and selectivity, but also exceptional temporal resolution. Previously, existing ACh biosensors were limited to response times on the order of second or sub-seconds, which is far too slow to resolve the fast kinetics of synaptic release. To address this challenge, our group developed ultrafast ACh biosensors by modifying carbon fiber disc microelectrodes (5 μm and 30 μm) with gold nanoparticles coatings and a monolayer of enzyme comprising acetylcholine esterase (AChE) and choline oxidase (ChO) [9,10]. This sensor design enabled sub-millisecond amperometric detection of ACh exocytosis by converting ACh into the electroactive reporter molecule, hydrogen peroxide (H_2O_2). Using these sensors, we characterized amperometric spikes that revealed the dynamics of vesicular fusion pore opening, lifetime and vesicle quantal content [10–12]. However, the relatively large sensor dimensions limited their use to extracellular exocytosis measurements near release sites located at tiny synapse and prevented intracellular access and direct quantification of vesicular ACh storage. To address this size limitation, we recently introduced a rapid, robust and easy-to-use droplet-etching method for fabricating short (~10 μm) carbon fiber nanotip electrodes (CFNEs) with reproducible distinct geometries [13]. The small, pointy shape with significantly lower electrode surface areas, provide low-noise, high spatial precision and minimal invasiveness, making these electrodes ideally suited for intracellular applications and synaptic recordings.

By integrating our ultrafast ACh biosensor design onto our needle-shaped CFNEs, we created a nanometric, low-noise ACh biosensor functionalized with gold nanoparticles and a monolayer of AChE:ChO enzyme coating [9,10,14]. This miniaturized biosensor enables dual functionality: (i) direct cytoplasmic insertion for quantifying vesicular ACh storage and (ii) extracellular placement at neuronal release sites for probing exocytotic ACh release with sub-millisecond resolution.

Despite recent technical advances, the intricacies of ACh release from differentiated SH-SY5Y cells remain poorly understood. A key question is whether vesicles undergo full or partial release during exocytosis, which is a process governed by the fusion pore dynamics. This distinction is biologically important, particularly for modeling disorders like Alzheimer's disease, where ACh signaling is disrupted.

To address this, direct intracellular measurements of vesicular ACh content are essential. Previous studies have shown that when nanoelectrodes are inserted into the cytoplasm, vesicles can adsorb and burst upon contact with the electrode held at constant potential, releasing their content for amperometric detection [15]. Applying this strategy with our needle-shaped ACh biosensor enables direct comparison between stored vesicular ACh and exocytotically released ACh, thereby providing insights into release efficiency and fusion pore behavior.

Using this approach, we quantified both intracellular vesicle ACh content and extracellular presynaptic exocytotic release from neurite terminals of differentiated human cholinergic SH-SY5Y cells. Paired analysis revealed that intracellular vesicle bursts contained, on average, 1.8-fold greater ACh content and exhibited a 1.2-fold higher mode value than exocytosis events. However, the most frequent intracellular vesicle bursts contained only about half as much ACh as higher-charge presynaptic exocytosis events. Together, these findings indicate that both intracellular vesicle bursts and synaptic exocytosis in differentiated SH-SY5Y cells predominantly proceed via partial release. This highlights the critical role of high-temporal resolution electrochemical tools in resolving fusion pore dynamics and establishes an important benchmark for using SH-SY5Y in disease-modeling.

2. Results and discussion

2.1. Fabrication of Ultrafast Needle-Shaped ACh Biosensors for Intracellular and Presynaptic Exocytotic Measurements in Differentiated Cholinergic SH-SY5Y Cells

To quantify intracellular ACh vesicle storage and compare it directly with exocytotic release, we constructed ultrafast enzymatic ACh biosensors on needle-shaped CFNEs. These sensors were specifically designed for high spatiotemporal resolution and minimal invasiveness, enabling both intracellular recordings and extracellular detection at presynaptic release sites of differentiated human cholinergic SH-SY5Y cells. These cells were selected as models because of their human origin, ease of culture, and suitability for cholinergic differentiation. As a human-derived, neuron-like model, differentiated SH-SY5Y cells offer a practical and promising physiologically relevant system for studying cholinergic release dynamics. Compared to iPSC-derived neurons, they provide a more accessible alternative for basic research and are suitable for probing the basic synaptic machinery underlying cholinergic transmission.

Needle-shaped CFNEs were fabricated using our previously established microscopy-aided electrochemical droplet etching method, yielding reproducible tips of ~100 nm diameter and ~ 10 μm length within ~2 min per electrode (Fig. 1A), as previously validated for analysis of dopamine-filled liposomes [13]. Building on this platform, and performing slight modifications to previous protocols [10,12], gold nanoparticle (AuNPs) were electrodeposited onto the needle-shaped CFNE surface to create a nanostructured surface optimized for enzyme immobilization. The electrode carbon tip was immersed in a 0.1 mM $HAuCl_4$ solution prepared in 0.5 M H_2SO_4 and two-step potential protocol was applied. First applying a 10 s potential step of +1.1 V (vs. Ag/AgCl) followed by a 4 s potential step at −0.6 V promoted AuNP nucleation and growth. Scanning Electron Microscopy (SEM) imaging analysis was used to confirm a uniform AuNP coating at the electrode surface (Fig. 1A). Image J software particle analysis ($n = 325$) revealed a

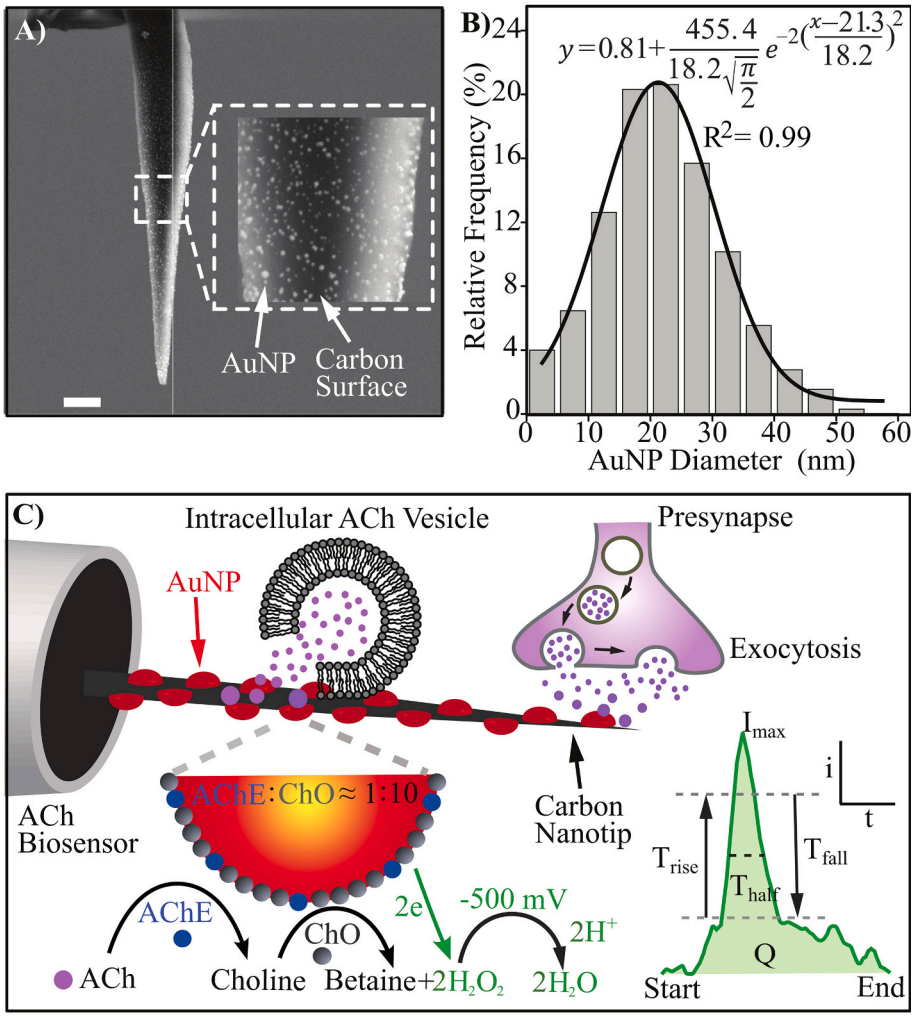

Fig. 1. Ultrafast acetylcholine (ACh) detection using an enzyme-functionalized, needle-shaped, carbon fiber nanotip electrode (CFNE). A) Scanning electron microscopy (SEM) image of a needle-shaped CFNE uniformly coated with electrochemically deposited gold nanoparticles (AuNPs). Scale bar is 1 μm. Inset shows a magnified view with a 100 nm scale bar. B) Histogram of AuNPs size distribution on the CFNE surface ($n = 325$ particles), fitted with a Gaussian function. (Bin size: 5 nm. C) Schematic of the ultrafast ACh biosensor and detection principle. The CFNE is modified with ~20 nm AuNPs (red hemispheres) and a molecular monolayer of enzyme composed of acetylcholinesterase (AChE, blue hemispheres) and choline oxidase (ChO, gray hemispheres) in a 1:10 ratio optimized for efficient catalytic conversion of ACh [14]. ACh released from intracellular vesicle burst or extracellular exocytosis is catalyzed by AChE to generate choline, whose oxidation is subsequently catalytically converted by ChO to produce hydrogen peroxide (H_2O_2). H_2O_2 is amperometrically detected by its electrochemical reduction reaction at −500 mV vs a chloridized Ag wire. The integrated area under the current signal, corresponding to the total charge (Q), is proportional to the ACh quantal size. The figure is not drawn to scale. The bottom right panel illustrates representative single-vesicle amperometric spike parameters: I_{max} (peak amplitude), $T_{1/2}$ (peak half-width), T_{rise} and T_{fall} (rise and decay times between 25% and 75% of I_{max}) and T_{base} (total spike duration). (For interpretation of the references to colour in this figure legend, the reader is referred to the web version of this article.)

Gaussian distribution with a mean AuNP diameter of 21 nm ($R^2 = 0.99$; bin size = 5 nm; Fig. 1B). These AuNPs provided a highly curved surface that served as an platform for enzyme attachment, prevented enzyme denaturation and enhanced the electrochemical detection of hydrogen peroxide [11]. Following our previously established design, a monolayer of enzyme composed of acetylcholinesterase (AChE) and choline oxidase (ChO) in an optimized 1:10 M ratio was immobilized onto the AuNP-modified CFNEs. The enzyme cascade selectively catalyzes ACh into electroactive hydrogen peroxide (H_2O_2), which is reduced and amperometrically detected at the potential of −500 mV vs. a chloridized Ag wire (Fig. 1C). Only biosensors exhibiting stable baselines and low noise were selected for subsequent cell measurements to ensure high-fidelity recordings.

2.2. Intracellular and Presynaptic Exocytosis Detection of ACh in Differentiated Cholinergic SH-SY5Y Cells

Human SH-SY5Y cells were differentiated to a cholinergic phenotype over 7 days through a sequential treatment using retinoic acid (RA) followed by brain derived neurotrophic factor (BDNF) as shown by the protocol in Fig. 2A [16]. Single-cell amperometric measurements were performed on days 8–9 using the CFNE ACh biosensor. For exocytosis measurements, the biosensor was gently positioned at the neurite terminals of differentiated cells (Fig. 2C), the primary site of regulated Ca^{2+}-triggered neurotransmitter release, where active-zone scaffolds support vesicle docking/priming and tight nanodomain clustering of Ca^{2+} channels to the Ca^{2+} sensor synaptotagmin [17,18]. Amperometric signals were recorded at a constant applied potential of −500 mV (vs. a chloridized Ag wire) and sampled at 100 kHz, revealing distinct current spikes (Fig. 2B). Each spike corresponds to an individual exocytosis

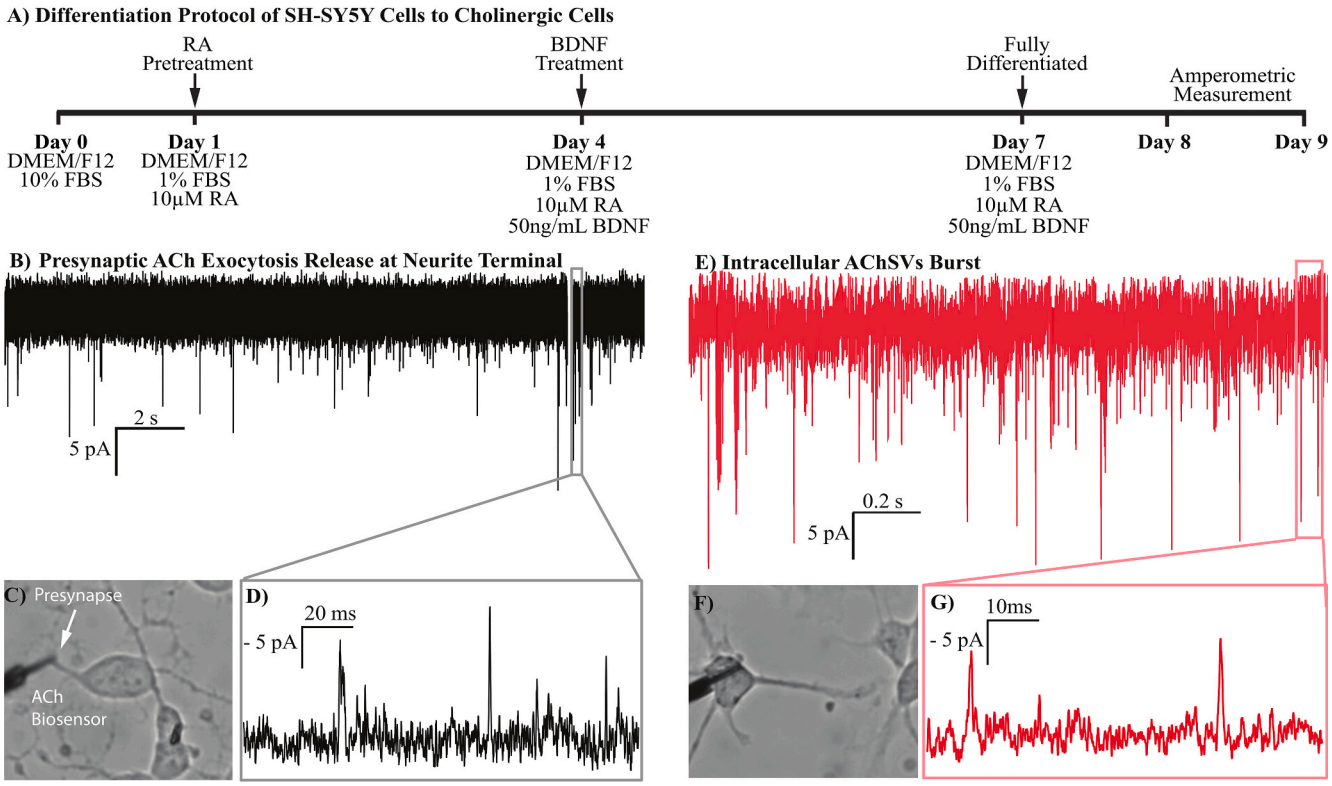

Fig. 2. Comparative amperometric analysis of presynaptic exocytosis ACh release and the vesicular ACh quantal content in differentiated human cholinergic SH-SY5Y cells using ultrafast ACh carbon fiber nanotip biosensors. A) Schematic illustration of the cholinergic differentiation protocol for SH-SY5Y human neuroblastoma cells. Cells were differentiated into a cholinergic phenotype over seven days using retinoic acid (RA), followed by treatment with brain-derived neurotrophic factor (BDNF). Single-cell amperometric measurements were performed on Days 8 and 9. B) Representative amperometric trace showing exocytotic ACh release events at neurite terminals (black). C) Microscopy image of the experimental setup for extracellular amperometric exocytosis recording using the CFNE biosensor. D) Magnified view of a single exocytotic spike from the trace shown in (B), demonstrating sub-millisecond resolution. E) Representative intracellular amperometric trace (red) showing ACh release synaptic vesicle (SV) bursts within the cell cytoplasm. F) Microscopy image showing intracellular insertion of the needle-shaped CFNE biosensor for quantification of vesicular ACh storage. G) Zoomed-in trace of an intracellular vesicle burst, showing spike resolution comparable to that of exocytotic events. All recordings were performed at a sampling rate of 100 kHz under a constant applied potential of −500 mV against a chloridized Ag wire. (For interpretation of the references to colour in this figure legend, the reader is referred to the web version of this article.)

event, and magnified traces demonstrate the sub-millisecond temporal resolution achieved (Fig. 2D). To assess intracellular vesicular ACh storage, the same biosensor was inserted directly into the cytoplasm of the differentiated SH-SY5Y cells (Fig. 2F, Video S1). Because penetration of extremely thin neurite terminals with a rigid nanoscale electrode can lead to local membrane rupture, uncontrolled Ca^{2+} influx, and local degeneration of the injured neuronal segment [19,20], intracellular measurements were instead performed at the soma, which tolerates brief electrode insertion without compromising overall cell integrity. To confirm that intracellular insertion was minimally invasive, we performed cell morphology, functionality and membrane-integrity assessments (Fig. S3). Cells showed no visible morphology changes following nanosensor insertion, remained adherent and exhibited stable intracellular vesicle-burst activity for several minutes following nanosensor withdrawal. Importantly, the same cells could subsequently be used for exocytosis measurements at the same axon terminals. Trypan blue exclusion assays performed after sensor withdrawal showed no dye uptake, indicating preserved membrane integrity. These observations are consistent with previous studies demonstrating rapid membrane resealing and minimal perturbation following intracellular penetration with nanoscale electrodes of comparable dimensions [15,21].

Under identical experimental conditions, amperometric current spikes were successfully recorded (Fig. 2E-G). These intracellular spikes correspond to cytoplasmic vesicles adsorbing to the electrode surface and, in response to the applied potential, spontaneously bursting open, releasing their neurotransmitter content onto the sensor. This allows quantification of the vesicular ACh quantal content at the single-vesicle level. Together, these results confirm that our CFNE ACh biosensor achieves sub-millisecond temporal resolution comparable to traditional 5 μm disk biosensors [9], but uniquely with its ultrasmall size extends the capability to both intracellular environments and synapses. This dual functionality, recording both real-time vesicle pore opening and fusion dynamics at exocytotic release and intracellular vesicular storage, represents a significant advance in the electrochemical interrogation of cholinergic signaling and capturing.

2.3. Comparison of Intracellular ACh Vesicle Content and Presynaptic Exocytotic ACh Release in Differentiated Human Cholinergic SH-SY5Y Cells

Having established that our CFNE ACh biosensor can measure both exocytotic release and intracellular vesicle ACh content, we next performed a direct quantitative comparison to investigate the neurotransmitter release efficiency and kinetic release parameters in cholinergic SH-SY5Y cells. This is an essential approach for characterizing the nature of fusion pore-regulated quantal release, which has remained understudied despite its relevance for understanding human cholinergic signaling in health and disease. To eliminate sensor-to-sensor variability, exocytosis and intracellular measurements were performed using the same CFNE ACh biosensor for each individual cell recording. Data were collected from 14 differentiated cholinergic SH-SY5Y cells, yielding detection of 2266 exocytotic events and 1935 intracellular

vesicle-burst events. Analysis of mean values of quantitative and kinetic amperometric spike parameters (Fig. 1C) revealed that, compared with exocytotic spikes, intracellular events exhibited higher current amplitudes and larger integrated total charge (Q). The mean charge across 14 cells was approximately 6.6 fC for exocytotic events and 11.8 fC for intracellular measurements. In contrast, temporal parameters such as T_{rise}, T_{fall}, and $T_{1/2}$ remained similar and within the sub-millisecond range (Fig. 3A). Intracellular vesicle-burst spike features reflect vesicle rupture in the cytosol and therefore do not involve SNARE-regulated fusion-pore dynamics. Consequently, there is currently no validated morphological basis to reliably distinguish rupture of a single vesicle from coincident rupture of multiple vesicles within the cell. However, the intracellular burst events displayed relatively uniform sub-millisecond kinetics similar to liposome-burst events and previously reported exocytosis spikes (Wang et al., JACS 2024) [9], supporting the interpretation that most well-resolved intracellular spikes represent rupture of individual vesicles. Although overlapping intracellular vesicle-burst spike features cannot be excluded, all well-resolved intracellular vesicle-burst spikes were included in the quantal charge distributions. Therefore, our initial comparisons between intracellular and exocytotic measurements were based on average charge values (Fig. 3A). Comparing the average Q, reflecting the total amount of ACh released per vesicle, intracellular vesicle bursts of 11.8 fC were detected, which corresponded to 1.8-fold greater amount of ACh than the 6.6 fC measured during exocytosis. The similarity in spike kinetics across both conditions supports the interpretation that each spike represents a single-vesicle release event, while the difference in charge reflects that a greater amount of ACh is stored in vesicles compared to the amount released. Hence, the exocytosis data likely reflect fusion pore-regulated partial release events, commonly referred to as kiss-and-run exocytosis in these cells [22–24].

Representative averaged spikes illustrate this difference (Fig. 3B) where both exocytotic release events (n = 147 spikes, black) and intracellular vesicle burst events (n = 135 spikes, red) showed similar temporal characteristics, but intracellular spikes were larger in amplitude and displayed greater charge (Q). According to Faraday's law: $N = Q/nF$, where n is the number of electrons transferred per molecule going through a redox reaction (n = 2 for H_2O_2), F is the Faraday's constant (96,485C/mol), and N is the number of reporter molecules detected from one release event and Q is the charge from integrating the current of each single amperometric spike, this directly translates to a higher number of ACh molecules detected per vesicle in intracellular recordings via the enzymatically generated H_2O_2. However, it is important to note that absolute quantification using the formula is prone to error due to the dependence of the sequential enzymatic catalysis efficiency of ACh at the biosensor surface. Charge distribution analysis further reinforced this conclusion. Histograms of spike charge (Fig. 3C) for both exocytosis (2266 spikes, black) and intracellular (1935 spikes, red) measurements across 14 cells demonstrated with lognormal fitting that the mode charge from intracellular vesicle bursts was 3.3 fC versus 2.8 fC for exocytosis events, indicating a 1.2-fold larger amount of ACh stored in vesicles than being released during exocytosis. Both exocytotic and intracellular quantal charge distributions were right-skewed, consistent with the log-normal fits shown in Fig. 3C. This skewness reflects the presence of a tail of larger-amplitude events in each dataset. Because these distributions were non-Gaussian, comparisons were performed using nonparametric statistics. A Kolmogorov–Smirnov test showed a significant difference between the cumulative distributions (D = 0.1989, $p < 0.0001$). Consistently, a Mann–Whitney U test indicated that intracellular quantal charge values (median = 6.467 fC) were statistically higher than exocytotic values (median = 4.466 fC; U = 1,599,451, p < 0.0001), with a Hodges–Lehmann median difference = 1.798 fC. Together, these results indicate that intracellular vesicle content is statistically higher than the quantal release measured during exocytosis. To further explore this, the cube root-transformed charge distributions were analyzed and fitted with Gaussian function, which confirmed the

A) Kinetic Parameters of Amperometric Spikes*

	T_{base}(ms)	$T_{1/2}$(ms)	T_{rise}(ms)	T_{fall}(ms)	I_{max}(pA)	Q(fC)
Exo	1.4 ± 0.1	0.5 ± 0.0	0.3 ± 0.0	0.3 ± 0.0	9.9 ± 1.7	6.6 ± 0.8
Intra	2.2 ± 0.2	0.7 ± 0.0	0.4 ± 0.0	0.6 ± 0.1	11.8 ± 1.8	11.8 ± 1.2

* Mean ± SEM (standard error of the mean)

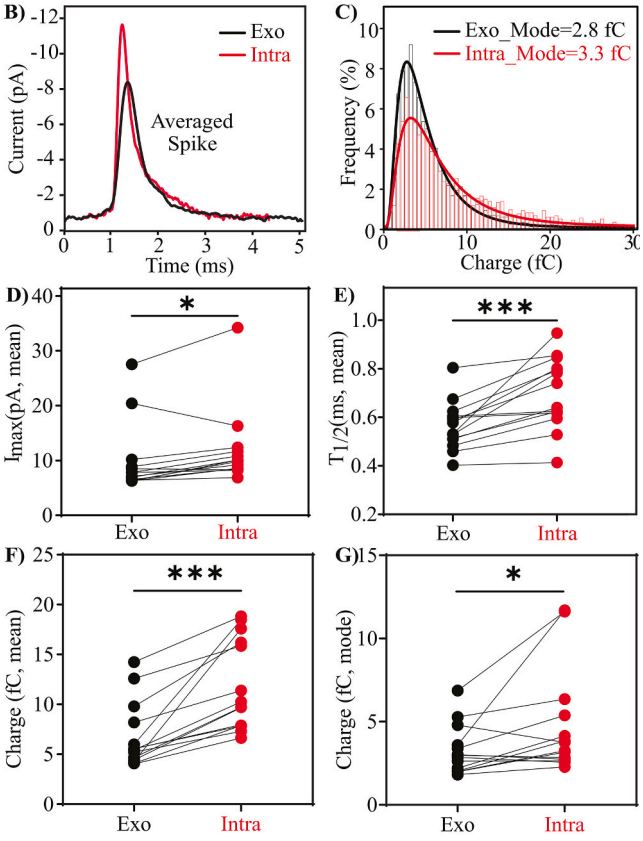

Fig. 3. Comparative analysis of acetylcholine (ACh) release during presynaptic exocytosis and intracellular measurements in differentiated human cholinergic SH-SY5Y cells. A) Summary of kinetic and quantitative parameters derived from amperometric spikes recorded during exocytotic (Exo, n = 2266 spikes) and intracellular (Intra, n = 1935 spikes) measurements. B) Averaged current spikes derived from 147 exocytosis events (black) and 135 individual intracellular synaptic vesicle bursts (red) recorded in the same cell with the same CFNE ACh biosensor. C) Normalized frequency histogram of quantal charge (Q) distributions for exocytosis (n = 14 cells, 2266 spikes, black) and intracellular vesicle bursts (n = 14 cells, 1935 spikes, red). A lognormal fit yielded mode values of 2.8 fC (R^2 = 0.99) and 3.3 fC (R^2 = 0.96) respectively (Bin size = 0.5 fC). The exocytotic and intracellular charge distributions differ significantly (Kolmogorov–Smirnov test: D = 0.1989, $p < 0.0001$; Mann–Whitney U test: U = 1,599,451, p < 0.0001; median exocytosis = 4.466 fC, median intracellular = 6.467 fC; Hodges–Lehmann median difference = 1.798 fC). D-G) Two-tailed paired comparisons of the mean kinetic and quantitative spike parameters: peak current (I_{max}, D, Wilcoxon test), half-width ($T_{1/2}$, E, t-test), and total charge (Q, F, Wilcoxon test) for exocytotic and intracellular measurements ($p <$ 0.001). G) Paired comparison of mode values of quantal charge derived from the lognormal fit of the histogram distribution. *$p < 0.05$, ***$p < 0.001$. "Exo" denotes exocytosis and "Intra" denotes intracellular measurements. All data were acquired from amperometric exocytosis measurements and intracellular vesicle content analysis recordings as matched pairs within the same cells using the same ACh biosensors (n = 14 pairs). (For interpretation of the references to colour in this figure legend, the reader is referred to the web version of this article.)

statistical significance of the shift (Fig. S1). Additionally, paired comparisons of key spike parameters (I_{max} and $T_{1/2}$) were performed across individual cells (Fig. 3D–E) and demonstrated statistically higher values for intracellular measurements ($n = 14$ cells; I_{max}, $p < 0.05$; $T_{1/2}$, $p < 0.001$), indicating a greater and more prolonged efflux of ACh per event. Consequently, the spike charge (Q), estimated from these parameters, was statistically higher for intracellular events (paired Wilcoxon test, n = 14 cells, p < 0.001; Fig. 3F). Together, these findings, derived from cell-averaged measurements and complementary statistical analyses, support the following interpretation. Only a fraction of vesicular ACh is released during exocytosis, consistent with a partial release mode, whereas intracellular vesicle bursting approximates the total detectable vesicle content. The predominance of partial release in cholinergic SH-SY5Y cells parallels observations from other cell types including PC12 cells, chromaffin cells and rodent glutamatergic synapses [15,25–27]. Additionally, the most frequent charge value (mode), estimated by fitting a lognormal distribution to the histogram (Fig. S2), was 1.2 times greater for intracellular recordings of ACh quantal size compared to the amount ACh released during exocytosis measurements (Fig. 3G).

The enzymatic nanobiosensor used here consists of a monolayer of AChE and ChOx assembled on a gold-nanoparticle–coated carbon-fiber nanotip electrode, with an effective diameter near the sensing region of ~1 μm. Over the 1–3 ms duration of a typical amperometric spike, ACh, choline, and H_2O_2 diffuse over distances of ~1–2 μm. This diffusion length is comparable to the nanosensor diameter and far greater than the ~7–10 nm thickness of the enzyme layer. Consequently, not all molecules released from a vesicle are captured and converted at the sensor surface. A fraction is expected to diffuse laterally away before undergoing enzymatic turnover. Such reaction–diffusion constraints are well known in enzymatic electrochemical systems. Incomplete conversion has been documented for multi-enzyme cascades on microelectrodes and predicted in theoretical treatments assuming a ~ 100 nm sensor–source separation [28,29]. Consistent with this, nanoscale vesicle-electrode modeling has shown that analyte loss occurs unless the vesicle pore opens very close to the electrode surface (Li et al., 2018) [30]. Our own simulations using a closely related nanotip geometry further support incomplete detection under realistic conditions [13]. Likewise, our prior liposome-based calibration using a gold-nanoparticle–coated carbon microelectrode inherently accounted for incomplete capture efficiency [9]. Therefore, the quantal charge measured here represents the effective detected vesicle content rather than the full vesicle load. In the present study, intracellular

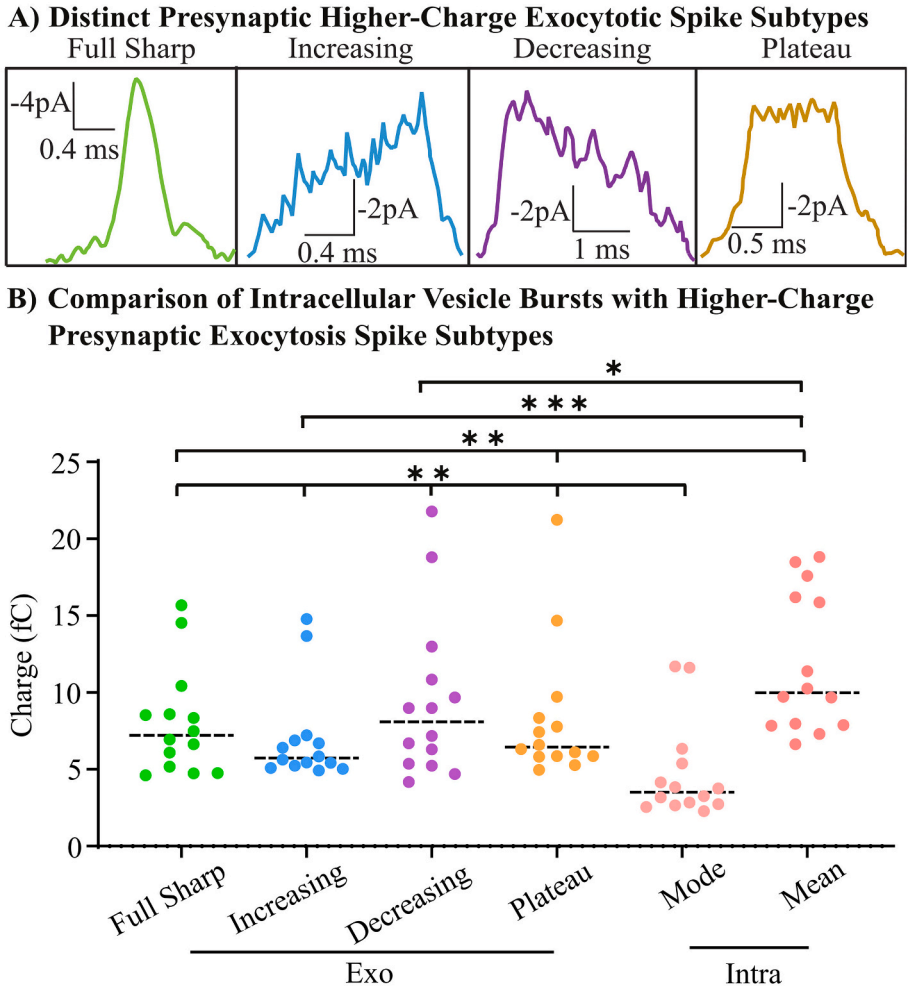

Fig. 4. Comparison of intracellular vesicle content and higher-charge exocytosis modes of ACh. (A) Representative amperometric spikes illustrating four distinct higher-charge exocytosis release modes, categorized by spike shape and duration: *full sharp (green)*, *increasing (blue)*, *decreasing (purple)*, and *plateau (orange)*. (B) Comparison of quantal charge across conditions. Detected charge values are compared among the four full-exocytosis release modes (full sharp, $n = 431$ spikes; increasing, $n = 187$ spikes; decreasing, $n = 152$ spikes; plateau, $n = 206$ spikes) and intracellular vesicle-burst measurement (mode, light pink; mean, dark pink; $n = 1935$). Each point represents the mean quantal charge (Q) calculated for an individual cell ($n = 14$ cells) for the indicated spike category. Dashed line indicates the median charge. Statistical analysis was performed using two-tailed Wilcoxon tests on paired measurements from 14 cells. *Exo* refers to exocytosis, and *Intra* refers to intracellular vesicle measurement. *$p < 0.05$; **$p < 0.01$; ***$p < 0.001$. (For interpretation of the references to colour in this figure legend, the reader is referred to the web version of this article.)

measurements involve vesicle rupture directly at the electrode surface, while exocytotic recordings are obtained with the electrode positioned in close proximity to the plasma membrane. Both measurement modes therefore operate under comparable reaction–diffusion constraints and use the same nanosensor architecture. Because our conclusions rely on the relative difference between intracellular and exocytotic charge distributions, rather than on absolute quantification, the finding that intracellular vesicle content exceeds exocytotically released charge remains robust despite finite detection efficiency.

2.4. Characterization of Presynaptic Exocytotic Spike Subtypes and Relative Quantal Release

To investigate the discrepancy between intracellular vesicle content and presynaptic exocytosis release, we selected the higher-charge exocytotic spike subtypes and classified them into four distinct release modes using our previously established criteria based on spike shape and duration [9,26]. Together, these subtypes account for approximately 40% of all detected exocytotic events, with each subtype representing roughly 7–15% of the total spike population. As shown in Fig. 4A, these included full sharp (green), increasing (blue), decreasing (purple) and plateau (orange) spikes, which reflect distinct fusion pore kinetic behaviors during exocytosis. Full-sharp spikes exhibit a simple monophasic waveform with a rapid rise followed by a slower decay, and typically show ~1.5-fold higher than those of the other spike types. This morphology is consistent with a rapidly formed fusion pore that undergoes an extensive dilation during the early phase of release, resulting in a larger amplitude than events with more restricted fusion-pore dilation. The term "full sharp," adopted from our previous classification, refers to spike morphology and does not denote complete release in this study. Increasing spikes display a prolonged rising phase followed by a sharp decay, consistent with gradual pore expansion before rapid closure, producing a characteristic prolonged rising limb of the spike. Decreasing spikes show a rapid onset followed by an extended decay, which is interpreted as an abrupt opening of the fusion pore that then partially constricts or relaxes more slowly, producing a decaying longer tail of the spike. Plateau spikes show a sustained peak current, reflecting a partly dilated stabilized fusion pore that remains open for an extended period before closing, generating a measurable plateau in the spike waveform. Importantly, these spike classes capture differences in fusion-pore kinetics, rather than full versus partial release on an event-by-event basis. Nevertheless, consistent with Wang et al., JACS 2024 [9], larger amplitude and higher-charge events (full-sharp, plateau, increasing, and decreasing) likely represent more dilated or longer-lived fusion-pore states, whereas the most frequent smaller sharp spikes (approximately 35%), are consistent with restricted and transient pore openings associated with partial ACh release. Together, this diversity in spike shapes highlights the dynamic nature of fusion-pore regulation as a major contributor to variability in quantal presynaptic neurotransmission, with may be an important regulatory feature in neuroplasticity.

The paired comparisons in Fig. 3G demonstrate that intracellular measurements yield higher quantal content than exocytosis events. Consistently, the mean intracellular charge in Fig. 4B (dark pink), exceeds that of each higher-charge exocytotic spike subtypes. Together, these findings indicate that even the larger-charge presynaptic exocytotic events at neurite terminals release less ACh than is detected in intracellular vesicle bursts, supporting the conclusion that synaptic exocytosis in these cells predominantly reflects partial neurotransmitter discharge. Although Fig. 4 focuses on the higher-charge exocytotic spike subtypes which together account for ~40% of all events, and are therefore not intended to represent the entire exocytotic distribution. Instead, the analysis examines whether these higher-charge spike subtypes approach the ACh vesicle content measured intracellularly. Importantly, the smaller sharp spikes remain the most abundant individual spike class (~35% of all events). When the entire spike population is considered in relation to intracellular vesicle bursts, exocytotic release in these cells predominantly reflects partial neurotransmitter discharge.

Notably the intracellular mode charge (light pink, Fig. 4B), representing the most frequent intracellular events is lower than both its mean value and the mean charge of each higher-charge exocytotic spike subtype. This difference likely reflects biological heterogeneity in vesicle content together with incomplete detection efficiency under intracellular bursts, where several factors, including vesicle rupture orientation, local diffusion dynamics, and nanosensor-vesicle contact geometry influence how much of the vesicle content is detected. For example, ACh released during rupture may diffuse away from the biosensor surface before complete enzymatic conversion [31], especially if vesicles rupture asymmetrically or away from the sensor surface. In addition, the macromolecularly crowded intracellular environment may further limit diffusion compared to extracellular recordings. Biological heterogeneity may also contribute, since vesicles at different stages of the exocytosis–endocytosis cycle, e.g. following transient kiss-and-run fusion or during vesicle refilling, may contain variable ACh loads [32]. However, intracellular measurements cannot distinguish true vesicle-to-vesicle differences in ACh content from variability caused by vesicle–electrode geometry and diffusion-limited detection that limit capture and enzymatic conversion at the nanosensor. Moreover, during intracellular positioning, occasional contact between the nanosensor and the plasma membrane could allow detection of membrane-proximal exocytotic events, which cannot be reliably separated from intracellular vesicle burst signals. Finally, Zhang's team showed that partial vesicle content release behavior also can occur in liposome systems via fusion pore flickering at the electrode surface, indicating that incomplete discharge can occur even in simplified model systems [33]. Therefore, while the nanoscale dimensions of the CFNE biosensor help mitigate these issues, the complex diffusion and fusion dynamics at the cell surface may still impose limitations on signal capture and interpretation. Taking together, these considerations further support the conclusion that partial release is the predominant mode of ACh exocytosis in differentiated cholinergic SH-SY5Y cells, while also explaining why intracellular rupture signals may underestimate the full vesicle load on an event-by-event basis.

2.5. Impact of Measurement Order on ACh Exocytosis and Intracellular Vesicle Quantal Content

Intracellular recordings consistently revealed higher quantal ACh content than exocytosis measurements. Previous studies have shown that perturbation to cell membrane can trigger and alter exocytosis through stress-triggered partial release in non-synaptic cells. For example, Chen et al. demonstrated that poking astrocytes with a glass micropipette induces calcium waves and 'kiss-and-run' glutamate exocytosis release, revealing a mechanosensitive release mechanism in glial cells [34]. Nan et al. used carbon-fiber nanotip electrodes to show that mechanical stress during intracellular penetration of PC12 and chromaffin cells can trigger and alter partial exocytosis while the electrode remains inside the cell [35]. These findings prompted a systematic evaluation of whether membrane perturbation could affect exocytosis measurements. Specifically, the influence of measurement sequence on spike characteristics was assessed. Concerns included whether temporary membrane penetration using CFNE ACh biosensor during intracellular recording might significantly perturb the cell membrane, deplete vesicle stores, or alter vesicle pool organization, thereby affecting subsequent exocytosis. Alternatively, performing exocytosis measurements first might lead to vesicle consumption or activate feedback mechanisms that alter intracellular vesicle content.

To address this, cells were divided into two groups in a total of 15 paired experiments: intracellular followed by exocytosis recordings ($n = 7$ cell pairs) and exocytosis followed by intracellular recordings ($n = 8$ cell pairs). For each pair, the ratio of intracellular to exocytosis values for I_{max}, $T_{1/2}$ and Q was compared across the two experimental orders.

As shown in Fig. 5, no significant differences were observed between the experimental orders. These results indicate that the sequence of measurements did not significantly affect the quantal characteristics of ACh release. This suggests that, in our experimental context, the temporary mechanical penetration of somatic membrane by the needle-shaped nanotip electrode, followed by its removal prior to exocytosis measurements at the axon terminals, may not induce sufficient long-lasting changes to the plasma membrane or vesicle pools at the axon terminals to affect their synaptic quantal release properties. Additionally, the prior exocytosis at the axon terminals did not significantly affect quantal release behavior of vesicles during intracellular bursting inside the soma. Several key distinctions likely explain the absence of measurement-order effects in our study. First, in our design, intracellular measurements were completed before exocytosis recordings, and the nanotip electrode was removed from the cell body prior to the latter, not causing sustained mechanical stress on the cell membrane. Second, in our experiments, intracellular vesicle measurements were performed at the soma, whereas exocytotic release was detected at axon terminals, spatially separating the sites of potential perturbation. The previous studies by Chen et al. and Nan et al., by contrast, conducted both measurements at the cell body [34,35]. Third, our use of differentiated SH-SY5Y cells, which form complex neuron-like networks, differs significantly from the non-neuronal secretory cells used in prior studies. These neuronal-like cells may possess more effective mechanisms for membrane repair and regulation, potentially mitigating any transient disruption from electrode insertion. Together, these factors likely contributed to the robustness of our dual-measurement protocol and the absence of recording-order-dependent effects on quantal ACh release.

This finding supports that our CFNE biosensor provides robust, reproducible and minimally invasive recordings across these experimental conditions. Importantly, the ability to perform paired intracellular and extracellular amperometric measurements in the same cell using the same biosensor offers a unique opportunity. This approach allows direct quantification of vesicle neurotransmitter loading versus release efficiency while controlling the biological variability and sensor-to-sensor variability, thereby strengthening the reliability of our conclusions.

3. Conclusions

In this study, we developed a robust, ultrafast enzymatic ACh biosensor by miniaturizing our previous micrometer-scale design into short needle-shaped carbon fiber nanoscale biosensors. The combination of dense AuNP functionalization and monolayer enzyme coatings enabled high catalytic efficiency, low-noise and sub-millisecond temporal resolution, allowing reliable detection of single-vesicle ACh release. Using differentiated human SH-SY5Y cells as a model of cholinergic neurons, this study established a methodology for paired, quantitative measurement of intracellular vesicular ACh storage and its release during exocytosis in the same differentiated cholinergic SH-SY5Y cell using the same single nanotip biosensor. Comparative analysis revealed that vesicles contain statistically higher ACh than is released during exocytotic, supporting the conclusion that partial release is the predominant exocytosis mode in these cells. By enabling minimally invasive, quantitative analysis of vesicular ACh storage and release kinetics at the single-vesicle level, this platform provides new insights into the regulation of cholinergic neurotransmission. More broadly, our biosensor technology provides a path to interrogate neurotransmitter dynamics within nanoscale cellular domains and to advance understanding of molecular mechanisms underlying neurodegenerative disorders involving cholinergic dysfunction, such as Alzheimer's disease.

4. Methods

4.1. Fabrication of Needle-Shaped CFNEs

Needle-shaped carbon fiber nanotip electrodes (CFNEs) were fabricated by electrochemically etching 5 μm in diameter cylindrical carbon fiber microelectrodes, prepared as previously described, into short (~10 μm) needle-shaped electrodes using a step-by-step controlled droplet-etching protocol with real-time optical monitoring [13].

Briefly, a single 5 μm carbon fiber was inserted into a borosilicate glass capillary (1.2 mm O.D., 0.69 mm I.D., Sutter Instrument Co., Novato, CA) and pulled using a micropipette puller (Model P-1000, Sutter Instrument Co., Novato, CA) to form a tapered glass tip. The excess carbon fiber extending from the taper was trimmed to ~50 μm and sealed with epoxy resin (EpoTek 301, Epoxy Technology, Billerica, MA). Electrodes were cured overnight at 100 °C (VENTICELL oven, MMM Medcenter Einrichtungen GmbH, Munich, GE).

Electrochemical etching was performed under an inverted microscope (Leica DM IRB, Leica Camera AG, Wetzlar, GE) using a 40× magnification objective and monitored in real-time via a digital GigE Vision camera (Manta G-235B ASG, ALLIED Vision Technologies GmbH, GE) that projected the process onto a computer screen for precise real-

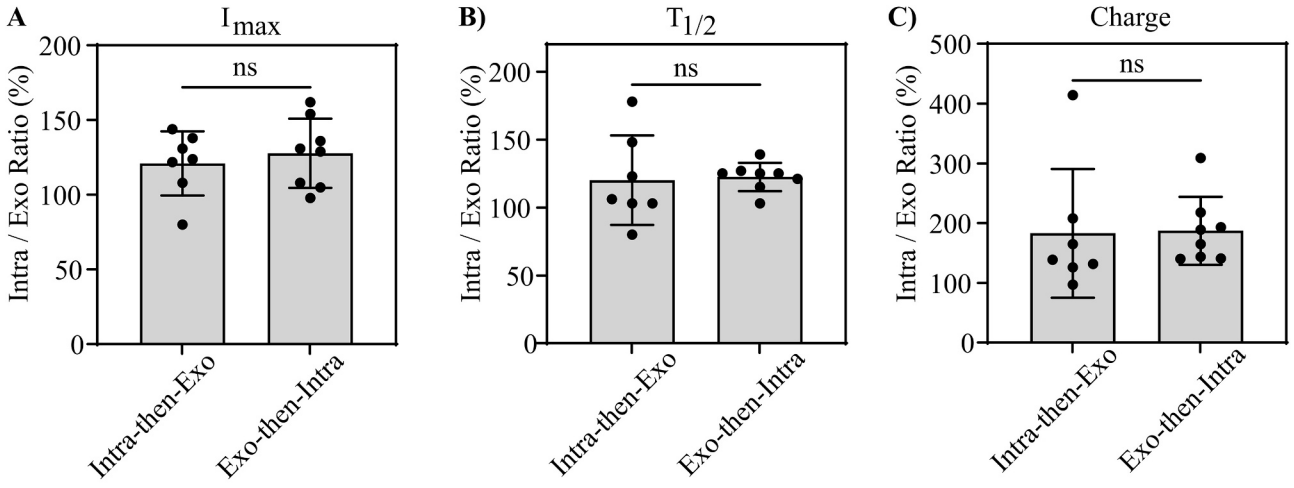

Fig. 5. Effect of experimental order on amperometric recordings of acetylcholine (ACh) release. A)-C) Comparison of spike parameters: peak current (I_{max}, A), half-width ($T_{1/2}$, B) and quantal charge (Q, C) obtained from intracellular vesicle content analysis (2108 spikes) and extracellular exocytosis recordings (2426 spikes). Data were collected in two experimental sequences: intracellular measurements followed by exocytosis recordings (n = 7 cell pairs) or exocytosis recordings performed before intracellular measurements (n = 8 cell pairs). Each point represents data from one matched cell pair recorded using the same ACh biosensor.

time observation. A 30 μL droplet of 4 M KOH was placed on a microscope slide and served as the etching medium. Both a silver wire reference electrode and the exposed carbon fiber tip were immersed into the droplet and connected to a constant voltage stimulator (DS2A - Mk.II model, Digitimer Ltd., UK) which delivered single voltage pulses for stepwise etching. The fiber was etched in three sequential voltage steps to gradually reduce its diameter and sharpen the tip: initially 4 V pulses were applied to reduce the diameter from 5 μm to ~2.5 μm, followed by 3 V pulses to narrow it further to ~1 μm and 2–2.5 V for final sharpening of the tip. This process produced reproducible, needle-shaped electrodes ~10 μm in length with a tip diameter of ~100 nm. The entire etching process required ~2 min per electrode. Throughout the procedure, care is taken to keep the glass–carbon junction near the air–liquid interface of the etching droplet to avoid damage and preserve the electrode tip's structural integrity.

Real-time monitoring also enabled electrode quality control: the appearance of air bubbles at the glass–carbon epoxy seal during etching indicates that the seal is not sufficient and such damaged electrodes were discarded. All etched CFNEs underwent quality assessment via cyclic voltammetry (CV) in a 1 mM ferrocenemethanol (FcMeOH) solution prepared in 100 mM KCl to ensure excellent electrochemical functionality. CVs were recorded between −0.2 V and + 0.8 V versus a saturated Ag/AgCl reference electrode (CH Instruments, USA) at a scan rate of 0.1 $V{\cdot}s^{-1}$. Only electrodes that displayed stable and well-defined redox responses were selected for subsequent gold nanoparticle (AuNP) deposition and biosensor fabrication.

4.2. Creation of Ultrafast Nanotip ACh Amperometric Biosensors

Ultrafast acetylcholine (ACh) biosensors were fabricated by functionalizing needle-shaped CFNEs with electrodeposited AuNPs followed by immobilization of a molecular monolayer layer of sequential enzymes comprising acetylcholinesterase (AChE) and choline oxidase (ChO). This approach was adapted from a previously established protocol in our lab with modifications [9,10,14].

To electrodeposit AuNPs, freshly etched CFNEs were immersed in 0.1 mM $HAuCl_4$ in 0.5 M H_2SO_4, together with a Ag/AgCl reference electrode. Using a potentiostat (Model 650 A Series Multi-Potentiostat, CH Instruments, Austin, TX, USA), a potential of +1.1 V was applied for 10 s followed by a step to −0.6 V for 4 s to promote uniform AuNP growth. This deposition method produced a dense and uniform AuNP coating, which enhanced electrode conductivity and sensitivity towards H_2O_2 detection, the electroactive reporter of enzymatic ACh breakdown.

To estimate the total gold surface area of the AuNP-modified CFNEs, a method based on Finot et al. was employed. The AuNP-coated electrode was immersed in 0.5 M H_2SO_4, and a potential of +1.4 V was applied for 5 s versus a $Cu/CuSO_4$ reference electrode [10], followed by a linear sweep from +1.4 V to +0.4 V at a scan rate of 0.1 $V{\cdot}s^{-1}$. The charge under the gold oxide reduction peak near +0.8 V was integrated and converted to the surface area, using a charge density constant of 489 $\mu C{\cdot}cm^{-2}$ [36].

The final step involved enzyme immobilization. AChE and ChO were co-immobilized onto the AuNP-coated surface by self-adsorption using a freshly prepared solution containing the AChE and ChO enzymes in a 1:10 M ratio, dissolved in 50 mM sodium phosphate buffer (pH 7.4). Each AuNP-coated electrode tip was immersed in 200 μL of this solution for 2–3 h at room temperature in the dark, forming a monolayer of enzyme coating enabling rapid sequential enzymatic conversion of ACh.

Biosensors were either used within 6 h of fabrication or stored at 4 °C in 50 mM sodium phosphate buffer (pH 7.4) for up to one day. Only biosensors passing strict quality control criteria including stable baseline, low noise, and absence of abnormal current transients in cell recording solution were selected for amperometric recordings.

4.3. Scanning Electron Microscopy of AuNPs-Coated Nanotip Electrodes

The AuNP deposition protocol was optimized and AuNP-modified CFNEs were characterized using a field emission scanning electron microscope (FE-SEM, JEOL JSM-7800F Prime, JEOL GmbH, Germany). Prior to imaging, each electrode was backfilled with silver paste and a silver wire to establish a stable electrical connection. After the silver paste was completely dry, the electrodes were securely mounted on the SEM sample stage using both carbon and copper tape for proper grounding. High-resolution images were acquired to assess CFNE geometry and provide images on the density and size of the electrodeposited AuNPs.

4.4. Differentiation of Human Cholinergic Cells

SH-SY5Y human neuroblastoma cells (ECACC 94030304) were cultured in DMEM/F12 medium supplemented with 10% fetal bovine serum (FBS) and GlutaMAX™. The culture medium was replaced every two days. Cells were maintained at 37 °C in a humidified atmosphere with 5% CO_2 and passaged upon reaching 80% confluency.

To generate cholinergic cells capable of releasing acetylcholine for amperometric measurements using the ACh biosensor, SH-SY5Y cells were differentiated into a cholinergic phenotype following the protocol described by de Medeiros et al., with minor modifications [16]. Briefly, undifferentiated SH-SY5Y cells were seeded at a density of 5000 cells/cm^2 onto 35 mm MatTek dishes with glass coverslip bottoms (MatTek, Ashland, MA, USA), pre-coated with poly-L-ornithine and Biolaminin 521 (BioLamina AB, Sundbyberg, Sweden) in DMEM/F12 containing 10% FBS.

On the following day, the medium was replaced with DMEM/F12 supplemented with 1% FBS and 10 μM retinoic acid (RA) to initiate cholinergic differentiation. After four days of RA pre-treatment, the medium was changed to DMEM/F12 containing 1% FBS, 10 μM RA, and 50 ng/mL brain-derived neurotrophic factor (BDNF; PreproTech, Cranbury, NJ, USA). The cells continued to differentiate for an additional 4–5 days (Days 8–9) before being used for amperometric measurements and imaging.

4.5. Amperometric Measurements of Presynaptic ACh Exocytosis and Intracellular Quantal Vesicle Content in Differentiated Human Cholinergic Cells

Amperometric recordings of ACh exocytosis and intracellular vesicle content were performed on differentiated human cholinergic cells between days 8–9 of differentiation, as described previously [9]. Freshly prepared ultrafast ACh nanotip biosensors were used for all measurements.

Cells were cultured in 35 mm MatTek glass-bottom dishes and rinsed three times with pre-warmed isotonic HEPES buffer saline (10 mM HEPES, 2 mM $CaCl_2$, 1.2 mM $MgCl_2$, 5 mM glucose, 150 mM NaCl, 5 mM KCl, pH 7.4). Approximately 2 mL of the same buffer was added to the dish for recordings, with additional volume supplied as needed to compensate for evaporation.

Recordings were performed on a Leica DM IRB inverted microscope (Leica Microsystems, Wetzlar, Germany) equipped with a stage heater (Bioscience Tools, San Diego, CA, USA) to maintain a temperature of ~31 °C in the region containing the cells. All biosensors were quality tested and only those with stable baselines and no aberrant current fluctuations were selected for recordings. For regulated presynaptic exocytosis release recordings, the ACh biosensor was gently positioned near the neurite terminal of a single cell using a micromanipulator (Scientifica, East Sussex, UK). For intracellular recordings of vesicle ACh quantal content, the biosensor tip was brought near the soma membrane (at the neurite-origin region) and carefully inserted into the cytoplasm by slowly penetrating the membrane to minimize mechanical damage and avoid triggering necrosis (Video S1). Here, the term “vesicle burst”

refer to the rupture of a single vesicle at the nanoelectrode surface, producing a single amperometric spike."

All biosensor placement procedures were performed under optical guidance using microscope objectives ranging from 10× to 40×. A constant potential of −0.5 V versus a chloridized Ag wire reference electrode was applied to the biosensor surface via an ultra-low noise patch clamp amplifier (Axopatch 200B, Molecular Devices, San Jose, CA, USA) connected to a low-noise digitizer (Digidata 1550B, Molecular Devices, San Jose, CA, USA) which was used to record amperometric signals at a sampling rate of 100 kHz with a 1 kHz low-pass Bessel filter applied via the potentiostat's internal circuitry. All measurements were conducted with the microscope heater turned off and within a Faraday cage to minimize environmental electrical noise.

4.6. Analysis of Amperometric Data

Data from amperometric recordings were analyzed using IgorPro software (versions 6.37 and 9, WaveMetrics, Lake Oswego, OR, USA), with the assistance of an Igor Procedure File developed by David Sulzer's lab for amperometric single-spike analysis [37]. Raw traces were smoothed using a binomial filter at 5 kHz. Spikes were considered valid if their peak current amplitude exceeded five times the standard deviation of the baseline noise. All detected spikes were manually examined to exclude false positives.

The following parameters were extracted from each spike from the analysis: T_{rise} and T_{fall}, representing the rise and fall times between 25% and 75% of the peak amplitude, respectively. $T_{1/2}$, referring to the spike width at half-maximal current. I_{max} is defined as the maximum peak current, and Q represents the total charge per spike, calculated by integrating the area under the current peak. These parameters were used to quantitatively compare the characteristics of ACh release events from intracellular and extracellular locations.

Supplementary data to this article can be found online at https://doi.org/10.1016/j.bioelechem.2026.109260.

CRediT authorship contribution statement

Yuanmo Wang: Writing – review & editing, Writing – original draft, Investigation, Formal analysis, Data curation, Conceptualization. **Ajay Pradhan:** Writing – review & editing, Methodology, Data curation, Conceptualization. **Pankaj Gupta:** Formal analysis, Data curation. **Jörg Hanrieder:** Resources. **Henrik Zetterberg:** Supervision, Resources. **Ann-Sofie Cans:** Writing – review & editing, Supervision, Resources, Project administration, Funding acquisition, Conceptualization.

Declaration of competing interest

The authors declare that they have no known competing financial interests or personal relationships that could have appeared to influence the work reported in this paper.

Acknowledgements

The authors gratefully acknowledge the use of the SEM instrument provided by the Chalmers Materials Analysis Laboratory (CMAL). We also thank Dr. Elin Esbjörner Winters for the use of the cell lab facility. This work was funded by The Swedish Research Council (VR-2020-04920), the Carl Trygger Foundation, the Chalmers Genie Initiative, and the Chalmers Nano Area of Advance. HZ is a Wallenberg Scholar and a Distinguished Professor at the Swedish Research Council supported by grants from the Swedish Research Council (#2023-00356, #2022-01018 and #2019-02397), the European Union's Horizon Europe research and innovation programme under grant agreement No 101053962, and Swedish State Support for Clinical Research (#ALFGBG-71320).

Data availability

Data will be made available on request.

References

[1] C. Sam, B. Bordoni, Physiology, Acetylcholine; StatPearls, 2022.
[2] B. Katz, R. Miledi, The statistical nature of the acetycholine potential and its molecular components, J. Physiol. 224 (3) (1972) 665–699, https://doi.org/10.1113/jphysiol.1972.sp009918.
[3] M.R. Picciotto, M.J. Higley, Y.S. Mineur, Acetylcholine as a neuromodulator: cholinergic signaling shapes nervous system function and behavior, Neuron 76 (1) (2012) 116–129, https://doi.org/10.1016/j.neuron.2012.08.036.
[4] Y.Y. Lim, P. Maruff, R. Schindler, B.R. Ott, S. Salloway, D.C. Yoo, R.B. Noto, C. Y. Santos, P.J. Snyder, Disruption of cholinergic neurotransmission exacerbates Abeta-related cognitive impairment in preclinical Alzheimer's disease, Neurobiol. Aging 36 (10) (2015) 2709–2715, https://doi.org/10.1016/j.neurobiolaging.2015.07.009.
[5] T.H. Ferreira-Vieira, I.M. Guimaraes, F.R. Silva, F.M. Ribeiro, Alzheimer's disease: Targeting the Cholinergic System, Curr. Neuropharmacol. 14 (1) (2016) 101–115, https://doi.org/10.2174/1570159x13666150716165726. Zhang, J.; Zhang, Y.; Wang, J.; Xia, Y.; Zhang, J.; Chen, L. Recent advances in Alzheimer's disease: mechanisms, clinical trials and new drug development strategies. Signal Transduction and Targeted Therapy 2024, 9 (1), 211. DOI: 10.1038/s41392-024-01911-3.
[6] V.G. Kesner, S.J. Oh, M.M. Dimachkie, R.J. Barohn, Lambert-Eaton Myasthenic syndrome, Neurol. Clin. 36 (2) (2018) 379–394, https://doi.org/10.1016/j.ncl.2018.01.008.
[7] K.L. Budzinski, R.W. Allen, B.S. Fujimoto, P. Kensel-Hammes, D.M. Belnap, S. M. Bajjalieh, D.T. Chiu, Large structural change in isolated synaptic vesicles upon loading with neurotransmitter, Biophys. J. 97 (9) (2009) 2577–2584, https://doi.org/10.1016/j.bpj.2009.08.032.
[8] J. Kovalevich, D. Langford, Considerations for the use of SH-SY5Y neuroblastoma cells in neurobiology, Methods Mol. Biol. 1078 (2013) 9–21, https://doi.org/10.1007/978-1-62703-640-5_2.
[9] Y.M. Wang, A. Pradhan, P. Gupta, J. Hanrieder, H. Zetterberg, A.S. Cans, Analyzing fusion pore dynamics and counting the number of acetylcholine molecules released by exocytosis, J. Am. Chem. Soc. 146 (38) (2024) 25902–25906, https://doi.org/10.1021/jacs.4c08450.
[10] J.D. Keighron, J. Wigstrom, M.E. Kurczy, J. Bergman, Y. Wang, A.S. Cans, Amperometric detection of single vesicle acetylcholine release events from an artificial cell, ACS Chem. Neurosci. 6 (1) (2015) 181–188, https://doi.org/10.1021/cn5002667.
[11] Y. Wang, R. Jonkute, H. Lindmark, J.D. Keighron, A.-S. Cans, Molecular crowding and a minimal footprint at a gold nanoparticle support stabilize glucose oxidase and boost its activity, Langmuir 36 (1) (2020) 37–46, https://doi.org/10.1021/acs.langmuir.9b02863.
[12] Y. Wang, D. Mishra, J. Bergman, J.D. Keighron, K.P. Skibicka, A.S. Cans, Ultrafast glutamate biosensor recordings in brain slices reveal complex single exocytosis transients, ACS Chem. Neurosci. 10 (3) (2019) 1744–1752, https://doi.org/10.1021/acschemneuro.8b00624.
[13] Y. Wang, P. Gupta, A. Pradhan, R. Trouillon, J. Hanrieder, H. Zetterberg, A.-S. Cans, Electrochemical droplet sculpturing of short carbon Fiber Nanotip electrodes for neurotransmitter detection, ACS Electrochemistry (2025), https://doi.org/10.1021/acselectrochem.5c00135.
[14] J.D. Keighron, S. Akesson, A.S. Cans, Coimmobilization of acetylcholinesterase and choline oxidase on gold nanoparticles: stoichiometry, activity, and reaction efficiency, Langmuir 30 (38) (2014) 11348–11355, https://doi.org/10.1021/la502538h.
[15] X. Li, S. Majdi, J. Dunevall, H. Fathali, A.G. Ewing, Quantitative measurement of transmitters in individual vesicles in the cytoplasm of single cells with nanotip electrodes, Angew. Chem. Int. Ed. Eng. 54 (41) (2015) 11978–11982, https://doi.org/10.1002/anie.201504839.
[16] L.M. de Medeiros, M.A. De Bastiani, E.P. Rico, P. Schonhofen, B. Pfaffenseller, B. Wollenhaupt-Aguiar, L. Grun, F. Barbe-Tuana, E.R. Zimmer, M.A.A. Castro, et al., Cholinergic differentiation of human neuroblastoma SH-SY5Y cell line and its potential use as an in vitro model for Alzheimer's disease studies, Mol. Neurobiol. 56 (11) (2019) 7355–7367, https://doi.org/10.1007/s12035-019-1605-3.
[17] T.C. Sudhof, The presynaptic active zone, Neuron 75 (1) (2012) 11–25, https://doi.org/10.1016/j.neuron.2012.06.012.
[18] E. Eggermann, I. Bucurenciu, S.P. Goswami, P. Jonas, Nanodomain coupling between ca(2)(+) channels and sensors of exocytosis at fast mammalian synapses, Nat. Rev. Neurosci. 13 (1) (2011) 7–21, https://doi.org/10.1038/nrn3125.
[19] Z. Bakaeva, M. Goncharov, I. Krasilnikova, A. Zgodova, D. Frolov, E. Grebenik, P. Timashev, V. Pinelis, A. Surin, Acute and delayed effects of mechanical injury on calcium homeostasis and mitochondrial potential of primary neuroglial cell culture: potential causal contributions to post-traumatic syndrome, Int. J. Mol. Sci. 23 (7) (2022), https://doi.org/10.3390/ijms23073858.
[20] P. Varier, G. Raju, P. Madhusudanan, C. Jerard, S.A. Shankarappa, A brief review of in vitro models for injury and regeneration in the peripheral nervous system, Int. J. Mol. Sci. 23 (2) (2022), https://doi.org/10.3390/ijms23020816.
[21] B.X.E. Desbiolles, E. de Coulon, A. Bertsch, S. Rohr, P. Renaud, Intracellular recording of cardiomyocyte action potentials with Nanopatterned volcano-shaped

microelectrode arrays, Nano Lett. 19 (9) (2019) 6173–6181, https://doi.org/10.1021/acs.nanolett.9b02209.
[22] G. Alvarez de Toledo, R. Fernandez-Chacon, J.M. Fernandez, Release of secretory products during transient vesicle fusion, Nature 363 (6429) (1993) 554–558, https://doi.org/10.1038/363554a0.
[23] T.A. Ryan, Kiss-and-run, fuse-pinch-and-linger, fuse-and-collapse: the life and times of a neurosecretory granule, Proc. Natl. Acad. Sci. USA 100 (5) (2003) 2171–2173, https://doi.org/10.1073/pnas.0530260100.
[24] A.A. Alabi, R.W. Tsien, Perspectives on kiss-and-run: role in exocytosis, endocytosis, and neurotransmission, Annu. Rev. Physiol. 75 (2013) 393–422, https://doi.org/10.1146/annurev-physiol-020911-153305.
[25] D.M. Omiatek, Y. Dong, M.L. Heien, A.G. Ewing, Only a fraction of quantal content is released during exocytosis as revealed by electrochemical cytometry of secretory vesicles, ACS Chem. Neurosci. 1 (3) (2010) 234–245, https://doi.org/10.1021/cn900040e.
[26] Y. Wang, H. Fathali, D. Mishra, T. Olsson, J.D. Keighron, K.P. Skibicka, A.S. Cans, Counting the number of glutamate molecules in single synaptic vesicles, J. Am. Chem. Soc. 141 (44) (2019) 17507–17511, https://doi.org/10.1021/jacs.9b09414.
[27] G.T. van Kempen, H.T. Vanderleest, R.J. van den Berg, P. Eilers, R.H. Westerink, Three distinct modes of exocytosis revealed by amperometry in neuroendocrine cells, Biophys. J. 100 (4) (2011) 968–977, https://doi.org/10.1016/j.bpj.2011.01.010.
[28] P. Lopes, K. Kaewjua, S. Shipovskov, E.E. Ferapontova, Glucose and glutamate detection by oxidase/hemin peroxidase mimic cascades assembled on macro- and microelectrodes, ChemElectroChem 11 (5) (2024) e202300682, https://doi.org/10.1002/celc.202300682.
[29] R. Dannaoui, I. Svir, W.-H. Huang, C. Amatore, A. Oleinick, Modeling the detection of transient vesicular exocytotic release from single cells with cylindrical enzymatic nanoelectrodes, Electrochim. Acta 508 (2024) 145214, https://doi.org/10.1016/j.electacta.2024.145214.
[30] X. Li, L. Ren, J. Dunevall, D. Ye, H.S. White, M.A. Edwards, A.G. Ewing, Nanopore opening at flat and Nanotip conical electrodes during vesicle impact electrochemical cytometry, ACS Nano 12 (3) (2018) 3010–3019, https://doi.org/10.1021/acsnano.8b00781.
[31] G.S. McCarty, L.E. Dunaway, J.D. Denison, L.A. Sombers, Neurotransmitter readily escapes detection at the opposing microelectrode surface in typical Amperometric measurements of exocytosis at single cells, Anal. Chem. 94 (27) (2022) 9548–9556, https://doi.org/10.1021/acs.analchem.2c00060.
[32] N.L. Chanaday, M.A. Cousin, I. Milosevic, S. Watanabe, J.R. Morgan, The synaptic vesicle cycle revisited: new insights into the modes and mechanisms, J. Neurosci. 39 (42) (2019) 8209–8216, https://doi.org/10.1523/jneurosci.1158-19.2019.
[33] S.T. Barlow, B. Figueroa, D. Fu, B. Zhang, Membrane tension modifies redox loading and release in single liposome Electroanalysis, Anal. Chem. 93 (8) (2021) 3876–3882, https://doi.org/10.1021/acs.analchem.0c04536.
[34] X. Chen, L. Wang, Y. Zhou, L.H. Zheng, Z. Zhou, "kiss-and-run" glutamate secretion in cultured and freshly isolated rat hippocampal astrocytes, J. Neurosci. 25 (40) (2005) 9236–9243, https://doi.org/10.1523/JNEUROSCI.1640-05.2005.
[35] X. Nan, M. Wang, J. Du, Y. Liu, L. Cao, J. Zhou, L. Liu, X. Li, Single vesicle chemistry reveals partial release happens at the mechanical stress-induced exocytosis, Talanta 271 (2024) 125637, https://doi.org/10.1016/j.talanta.2024.125637.
[36] M.O. Finot, G.D. Braybrook, M.T. McDermott, Characterization of electrochemically deposited gold nanocrystals on glassy carbon electrodes, J. Electroanal. Chem. 466 (2) (1999) 234–241, https://doi.org/10.1016/S0022-0728(99)00154-0.
[37] E.V. Mosharov, D. Sulzer, Analysis of exocytotic events recorded by amperometry, Nat. Methods 2 (9) (2005) 651–658, https://doi.org/10.1038/nmeth782.